HAL
open science

Local electrochemical impedance spectroscopy study of the influence of ageing in air and laser shock processing on the micro-electrochemical behaviour of AA2050-T8 aluminium alloy

Halina Krawiec, Vincent Vignal, Hassan Amar, Patrice Peyre

To cite this version:

Halina Krawiec, Vincent Vignal, Hassan Amar, Patrice Peyre. Local electrochemical impedance spectroscopy study of the influence of ageing in air and laser shock processing on the micro-electrochemical behaviour of AA2050-T8 aluminium alloy. Electrochimica Acta, 2011, 56 (26), pp.9581-9587. 10.1016/j.electacta.2011.01.091 . hal-02455210

HAL Id: hal-02455210

https://hal.science/hal-02455210v1

Submitted on 25 Jan 2020

HAL is a multi-disciplinary open access archive for the deposit and dissemination of scientific research documents, whether they are published or not. The documents may come from teaching and research institutions in France or abroad, or from public or private research centers.

L'archive ouverte pluridisciplinaire **HAL**, est destinée au dépôt et à la diffusion de documents scientifiques de niveau recherche, publiés ou non, émanant des établissements d'enseignement et de recherche français ou étrangers, des laboratoires publics ou privés.

Local electrochemical impedance spectroscopy study of the influence of ageing in air and laser shock processing on the micro-electrochemical behaviour of AA2050-T8 aluminium alloy

H. Krawiec[a], V. Vignal[b,*], H. Amar[b], P. Peyre[c]

[a] AGH, University of Science and Technology, ul. Reymonta 23, 30-059 Krakow, Poland
[b] ICB, UMR 5209 CNRS – Université de Bourgogne, BP 47870, 21078 Dijon, France
[c] LALP, Arts et Métiers Paritech, 151 Bd de l'Hopital, 75013 Paris, France

Keywords:
Aluminium alloy
EIS
Microstructure
Corrosion
Capillary techniques

A B S T R A C T

In the present paper, the micro-electrochemical behaviour of AA2050-T8 in 0.1 M NaCl was first studied after polishing by means of local electrochemical impedance spectroscopy and field-emission scanning electron microscopy/electron dispersive spectroscopy (FE-SEM/EDS). The influence of ageing in air and LSP was then investigated. Ageing in air for three months led to an increase in the charge transfer resistance. This was clearly observed in sites surrounding constituent particles where the charge transfer resistance was in the order of 1 MΩ cm^2 (instead of 10^{-3} MΩ cm^2 after polishing). Increased passivity around particles was confirmed from FE-SEM/EDS analysis. On the other hand, the effect of LSP on the behaviour of the matrix was found to be extremely beneficial. Both charge transfer and oxide film resistances were sharply increased to approximately 0.35 MΩ cm^2 and 1 MΩ cm^2, respectively, as opposed to approximately 1.9×10^{-3} MΩ cm^2 and 4.2×10^{-3} MΩ cm^2, respectively, after ageing in air. This was attributed to the presence of compressive stresses at the specimen surface after LSP treatment. Stress values were determined from XRD measurements.

1. Introduction

Aluminium alloys are a very important category of materials because of their high mechanical properties and wide range of industrial applications. It is well known [1–3] that aluminium alloys are prone to microstructural corrosion (pitting corrosion, intergranular corrosion, etc.). Microstructural corrosion is caused by the presence of intermetallic particles which may be either anodic or cathodic with respect to the matrix [1–4]. Micro-electrochemical techniques have been widely employed to obtain information about the role of particles in localised corrosion of aluminium alloys. pH microelectrode has been used [5] to demonstrate that alkalisation occurred around a synthetic Al_3Fe electrode coupled to a 6061 alloy sample in NaCl 0.6 M at pH 6.3. The local dissolution of various aluminium alloys has been probed *in situ* [6] in chloride solutions by using atomic force microscopy (AFM) and scanning electrochemical microscopy (SECM). Preferential dissolution in the boundary region between some intermetallic particles (IMPs) and the alloy matrix were observed during free immersion and under electrochemical anodic polarisation. The use of microcapillary cell techniques [7–10] has enabled the measurement of local breakdown potentials for areas in aluminium alloys containing one or a few intermetallics [11,12].

Surface modifications by LSP arise when surfaces are irradiated with nanosecond laser pulses that generate plasma-driven shock waves, which in turn lead to a certain amount of local plastic deformation. Thermal effects are avoided by covering the surface with an absorptive overlay which absorbs the laser beam (generally metal adhesive coatings). Deep (i.e. greater than 0.5 mm) and high-amplitude compressive residual stress fields, combined with relatively low work hardening rates (less than 20%) and limited roughening, are usually the main characteristics of surfaces having undergone LSP treatment. Considering previous results obtained on AA2024-T351 [13,14], LSP treatment is expected to bring about a combination of increased fatigue or wear resistance and improved corrosion behaviour. For example, it has been shown that the pitting potential is shifted to the anodic direction after LSP [14]. Such changes could be attributed to plastic deformation generated in the material during LSP.

Regarding the influence of mechanical stress on corrosion processes, limited research has been conducted on aluminium alloys. AA2024-T3 showed increased corrosion rates after prestressing [15], but little change in breakdown potentials. It was speculated that the increase in current density with increasing prestrain is

* Corresponding author. Tel.: +33 0 380396160; fax: +33 0 380396132.
E-mail address: vincent.vignal@u-bourgogne.fr (V. Vignal).

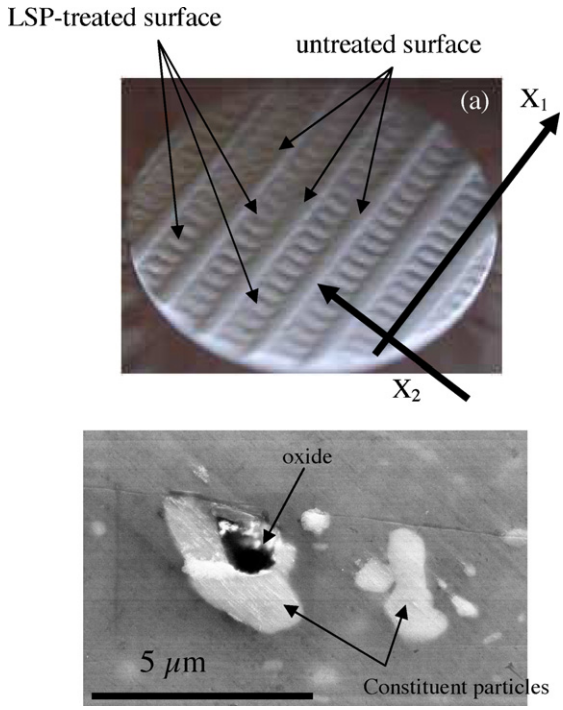

Fig. 1. (a) Optical image of the sample after LSP treatment. X_1- and X_2-axes used for stress measurements are indicated. (b) FE-SEM/EDS image of constituent particles in AA2050-T8 after mechanical polishing.

due to the deformation-induced defects. After straining in the plastic domain, a large amount of scatter was observed in the electrochemical response of an as-cast AlCu4Mg1 aluminium alloy [16]. The most active places corresponded to sites containing wide microcracks and severe damage in the matrix. In this case, the corrosion potential was approximately −1000 mV vs. Ag/AgCl, and the current in the passive domain was five times higher than that measured in the strained matrix. It was also found that the pitting potential was strongly affected by deformation processes.

In the present paper, the influence of LSP on the resistance to localised corrosion of AA2050-T8 is investigated in chloride media at the microscale by means of local electrochemical impedance spectroscopy and FE-SEM/EDS.

2. Experimental

2.1. Specimens and surface preparation

Experiments were performed on a 2050-T8 aluminium alloy (Cu: 3.73 wt.%; Li: 0.9%; Mg: 0.3%; Mn: 0.37%; Zr: 0.009% and Fe: 0.05%). Specimens were polished with silicon carbide (SiC) papers down to 4000 grit and smoothed with diamond pastes (9, 3 and 1 μm).

To prevent any thermal rise during LSP (and hence any microstructural changes), specimens were first covered with an 80 μm-thick metal adhesive coating. The specimen surface was then partially treated by LSP (Fig. 1(a)). Experiments were carried out with a frequency-doubled (0.532 μm) Nd:YAG laser capable of delivering up to 1.5 J in pulses of 9 ns duration at a 10 Hz repetition rate. 1.8 mm impact diameters were used to treat 1.5 cm circular areas. The intensity value was 3.5 GW cm^{-2}.

After LSP treatment, the surface was aged in air for three months. As the specimen surface was partially treated by LSP, it was possible to determine the effects of ageing in air on the untreated surface and deconvolute the effects of ageing in air from those of LSP treatment on the treated surface.

2.2. Local electrochemical measurements

Local electrochemical investigations were performed on the polished and LSP-treated surfaces using the electrochemical microcell technique [17]. The microcell was mounted on a microscope for precise positioning of the capillary at its surface. The capillary tip was adhered to the specimen surface with a layer of silicon rubber. Whenever the capillary was in contact with the specimen surface, elastic deformation of the silicon rubber was ensured. This method made it possible to perform measurements with extremely small capillaries (diameters less than 10 μm) [16]. In addition, the wetted area on the specimen could be calculated accurately using a specific image analysis procedure. Calculation of the current density could be validated by performing measurements with different capillary diameters and through numerical simulation [18,19]. All potentials were measured vs. Ag/AgCl (saturated solution) and the counter electrode was made of platinum wire.

Local electrochemical impedance spectroscopy (LEIS) data were obtained using glass capillaries with a diameter of 50 μm. LEIS diagrams were plotted in 0.1 M NaCl at 25 °C, after 25 min of immersion at the open circuit potential (steady state). An AutoLab PGZ32 electrochemical interface/frequency response analyser was used in these experiments. LEIS diagrams were plotted within a frequency range of 100 kHz to a few mHz (30 points) using 20 mV peak-to-peak sinusoidal potential difference.

Impedance data were fitted to the appropriate equivalent circuit using the Z-view software package. The first fitting was performed without any constraints. Parameters with a relative error of less than 5% were then fixed, and the fitting procedure was repeated. This method was applied until all the relative errors were smaller than 5%.

2.3. Surface observations and stress measurements at the microscale

A field emission scanning electron microscope (JEOL 6400F) with an integrated electron dispersion spectrometer (FE-SEM/EDS) was used to determine the morphology and chemical composition of constituent particles. The EDS analysis was performed on at least ten different sites, with 15 kV electron beam excitation (corresponding roughly to an approximate information depth of 1 μm).

Residual stresses (σ_{11} and σ_{22} along the X_1- and X_2-axes, respectively) were determined on the polished and LSP-treated surfaces using an X-ray θ/θ-type goniometer (D8 Discover with the General Area 2D Detector Diffraction System from Bruker AXS). The X-ray beam was focused using an aperture (diameter of 50 μm). Experiments were carried out on {3 1 1} planes using the $\sin^2\psi$ method [20]. The X-ray elastic constant was $1/2S_2 = 1.9 \times 10^{-5}$ MPa^{-1}.

3. Results and discussion

3.1. Microstructure

FE-SEM/EDS observations performed after polishing revealed the presence of constituent particles, as shown in Fig. 1(b). They were found to be Al–Cu–Mn–Fe-rich phase (Table 1), probably Al_7Cu_2Mn type particles with Fe substitution for some of the Mn. Their size was between 1 and 10 μm. Oxide particles were also detected (Fig. 1(b)). These particles contain oxygen (22.7 ± 2 at.%), aluminium (67.6 ± 0.4 at.%), copper (2.5 ± 1 at.%), iron (0.6 ± 0.6 at.%), manganese (1.4 ± 1.3 at.%) and silicon (5.1 ± 1.2 at.%). A small amount of scatter in the levels of alloying elements was obtained in oxide particles, indicating a homogeneous composition. The matrix, on the other

Table 1
Chemical composition of Al–Cu–Fe–Mn constituent particles (at.%).

	Al	Mn	Fe	Cu
Particle #1	68.7	3.7	6.3	21.4
Particle #2	74.6	2.5	5.0	17.9
Particle #3	70.0	1.7	6.2	22.2
Particle #4	69.5	2.7	6.6	21.3
Particle #5	79.5	1.9	4.2	14.4
Particle #6	68.4	2.8	6.8	22.0
Particle #7	69.7	3.6	6.1	20.7
Particle #8	71.0	2.6	6.3	20.2
Particle #9	72.8	1.8	5.8	19.6
Particle #10	79.3	1.3	4.4	15.0
Average values	72.3	2.8	6.3	19.5
Standard deviation	4.1	1.6	1.4	3.4

hand, was composed of aluminium (97.9 ± 0.09 at.%) and copper (2 ± 0.07 at.%). TEM analysis [21] performed on AA2050-T8 at the nanoscale showed that the main hardening phase is T1 (Al_2CuLi). The morphology of this phase is plate-like. The phase θ' was also present, but to a lesser degree. It has also been shown that Mn and Zr help to form an unrecrystallized structure, through precipitation as dispersoids (Mn and Al_3Zr dispersoids).

LSP treatment, which does not induce any thermal rise in the metallic alloy, had no influence on the size and chemical composition of constituent particles, hardening particles and oxides. No changes were also observed in the matrix composition.

3.2. Effect of LSP on surface morphology and residual stresses

Constituent particles were systematically situated higher than the matrix surface. The particle-matrix height difference was found to depend on the surface preparation. Values ranging from 100 to 200 nm and from 60 to 300 nm were obtained after mechanical polishing and after LSP treatment, respectively. This suggests that constituent particles underwent highly heterogeneous stresses during LSP. Most of these particles were pushed upwards with respect to the matrix surface level. Average values of residual stresses along the X_1- and X_2-axes (Fig. 1(a)) were determined from microXRD measurements. After LSP treatment, sites containing the matrix were found to be under compression ($\sigma_{11} = -165 \pm 40$ MPa and $\sigma_{22} = -160 \pm 30$ MPa). By contrast, extremely low stress values were registered after mechanical polishing: $\sigma_{11} = -30 \pm 30$ MPa and $\sigma_{22} = 15 \pm 25$ MPa.

AFM and FE-SEM/EDS observations of LSP-treated specimens revealed that some constituent particles were (partially or completely) debonded from the matrix. This resulted in the formation of cavities at the specimen surface, as shown in Fig. 2(a). Some microcracks were also detected in the matrix (Fig. 2(b)).

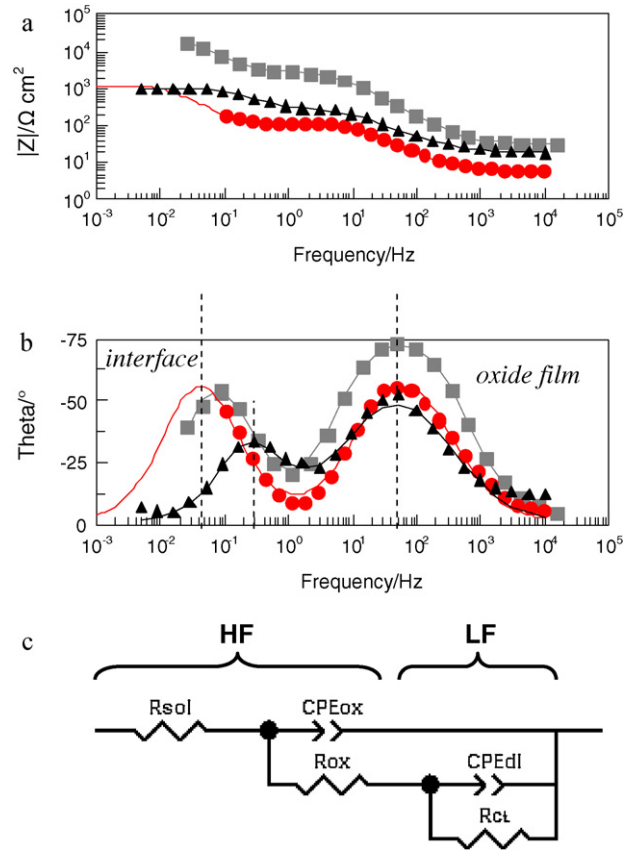

Fig. 3. (a, b) Global impedance diagram (Bode representation in grey squares). The lines represent the model data corresponding to the equivalent circuit in (c). Local electrochemical impedance diagrams obtained at sites containing the matrix (red circles) and the matrix with constituent particles (black triangles) are also shown. Experiments were conducted after immersion of AA2050-T8 in 0.1 M NaCl at the OCP value for 25 min using 50 μm diameter capillaries. (For interpretation of the references to color in this figure legend, the reader is referred to the web version of this article.)

3.3. Electrochemical impedance measurements after mechanical polishing

Electrochemical impedance measurements were first performed after mechanical polishing (reference curves). Global Bode diagrams exhibit two time constants, as shown in Fig. 3(a) and (b). This behaviour implies two different contributions. To identify these contributions, local impedance measurements were carried out in the matrix and in the matrix with constituent particles using small capillaries (50 μm in diameter), as shown in Fig. 3(a) and (b). It has been shown that the diffusive flux of species in the classical electrochemical cell is smaller than that in the electrochemical

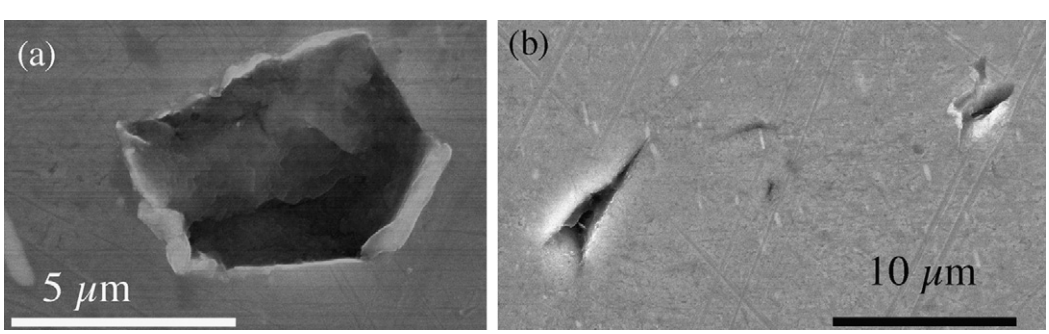

Fig. 2. FE-SEM/EDS images of surface defects generated by LSP treatment: (a) cavities and (b) microcracks.

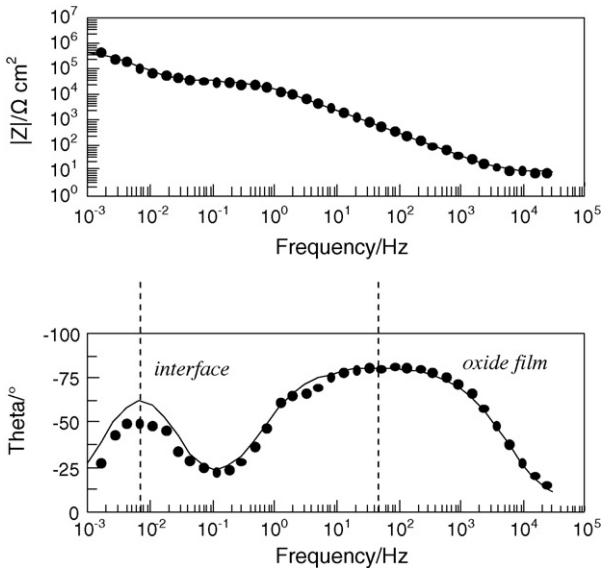

Fig. 4. Local impedance diagram (Bode representation) on pure aluminium. Experiments were conducted after immersion of aluminium in 0.1 M NaCl at the OCP value for 25 min using 50 μm diameter capillaries. The line represents the model data corresponding to the equivalent circuit in Fig. 3(c).

microcell [19], thereby resulting in higher current densities when using the electrochemical microcell technique. This explains the lower impedance values found at the microscale (Fig. 3(a) and (b)). Local electrochemical impedance measurements on AA2050-T8 were also compared to those obtained on pure aluminium (Fig. 4) using the same microcapillary diameter.

The capacitive loop at high frequencies was not altered by the presence of constituent particles. It has the same size and position both in sites containing the matrix and in those containing the matrix with constituent particles (Fig. 3(a) and (b)). It was also detected within the same frequency range on pure aluminium, suggesting that this contribution was not related to the hardening phase. The contribution at high frequencies was then associated with the oxide film that was formed on the matrix. The capacitive loop at high frequencies was larger on pure aluminium than on AA2050-T8. It has been shown that alloying elements have essential influence on the properties of the oxide film formed on aluminium alloys. Segregation of alloying elements (such as Mg in AA7075 [22] and tantalum in Al–Ta alloys [23]) may occur in the oxide film. It has been proposed [22,23] that local stresses may be generated by thermal expansion mismatch and composition gradients. These stress concentrations might affect the properties of the oxide layer in mechanical ways. In addition, the presence of the alloying elements (in the solid solution) might change the properties of the oxide layer in chemical ways. Therefore, differences in the shape of the capacitive loop at high frequencies between pure aluminium and AA2050-T8 might be explained by one of these assumptions. Further works are necessary to determine the origin of this finding.

By contrast, the presence of constituent particles and hardening phase gave rise to a shift in the second contribution towards higher frequencies (approximately 8 mHz on pure aluminium, Fig. 4, as opposed to approximately 40 mHz at sites containing the matrix with hardening phase and 200 mHz at sites containing the matrix with hardening phase and constituent particles, Fig. 3). This second contribution was associated with the charge transfer at the interface.

The equivalent circuit shown in Fig. 3(c) was used to describe the electrochemical behaviour of the alloy after mechanical polishing. R_{sol} is the solution resistance, R_{ct} is the charge transfer resistance at the interface and CPE_{dl} is the double layer CPE (constant phase

Table 2
Numerical values of the components used in the equivalent circuit for the fitting of experimental impedance diagrams.

	R_{el} ($\Omega\,cm^2$)	$CPE_{ox}-T$	$CPE_{ox}-P$	R_{ox} ($M\Omega\,cm^2$)	$CPE_{dl}-T$	$CPE_{dl}-P$	R_{ct} ($M\Omega\,cm^2$)
Global measurements AA2050	32.8	1.32×10^{-5}	0.93	3.07×10^{-3}	27×10^{-5}	1	0.02147
Local measurements (matrix of AA2050 after polishing)	7	1.49×10^{-4}	0.9	1.86×10^{-4}	8.2×10^{-3}	1	3.34×10^{-4}
Local measurements (matrix + precipitates of AA2050 after polishing)	17	1.65×10^{-4}	0.9	3.4×10^{-4}	1.82×10^{-3}	0.97	10^{-3}
Local measurements (matrix of AA2050 after ageing in air)	3.6	5.3×10^{-6}	0.9	1.92×10^{-3}	6.8×10^{-6}	0.94	4.23×10^{-3}
Local measurements (matrix + precipitates of AA2050 after ageing in air)	1.4	2.9×10^{-6}	0.96	2.95×10^{-3}	7.3×10^{-6}	0.95	1.7
Local measurements (matrix of AA2050 after LSP)	3.8	13.6×10^{-6}	0.87	0.34	37.5×10^{-6}	1	1
Local measurements (matrix + precipitates of AA2050 after LSP)	15	6.46×10^{-6}	0.85	2.84×10^{-3}	7.9×10^{-6}	0.94	0.7

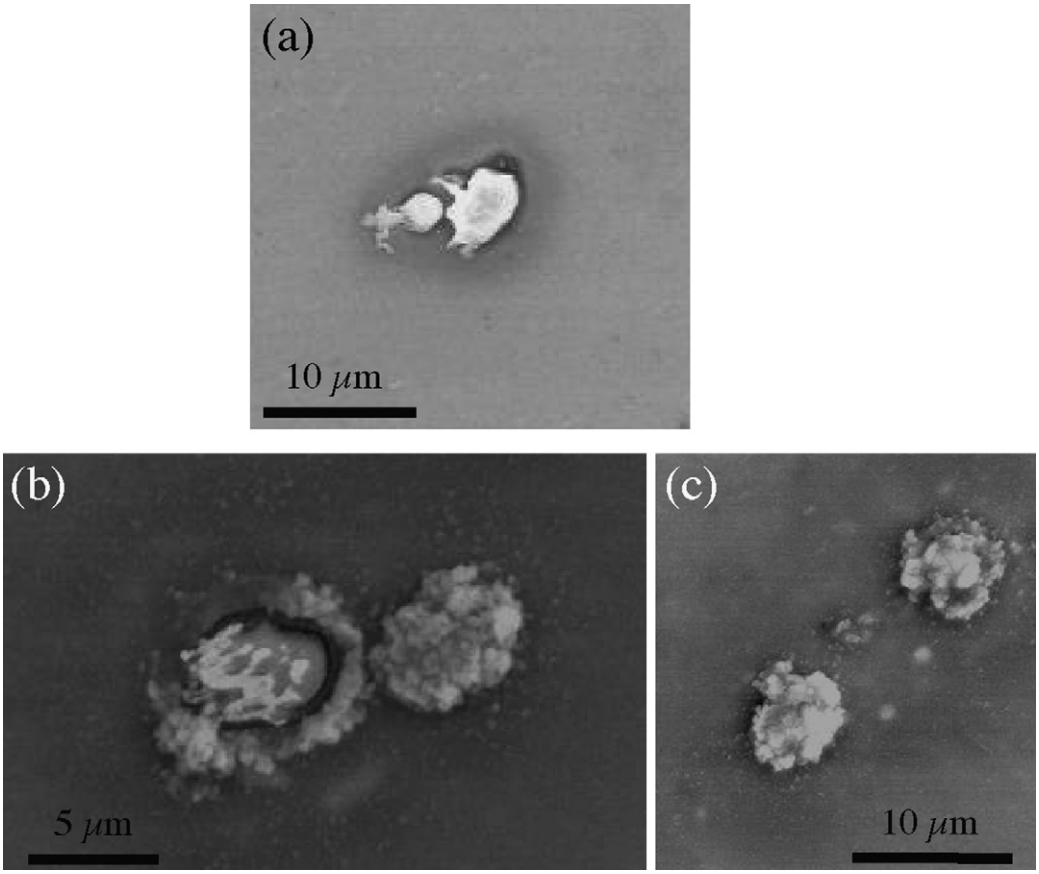

Fig. 5. (a–c) FE-SEM/EDS micrographs of sites with constituent particles after immersion in 0.1 M NaCl at OCP for 25 min.

element). The oxide film is considered to be a parallel circuit of a resistor due to the ionic conduction in the oxide film, and a capacitor due to its dielectric properties. R_{ox} is the oxide film resistance and CPE_{ox} is the CPE of the oxide film. The impedance of a CPE is defined as $Z_{CPE} = 1/T(j\omega)^{\varphi}$, where φ is the CPE exponent and T is the CPE coefficient. The numerical values used for each component are reported in Table 2.

The charge transfer and oxide film resistances were higher around constituent particles than in areas far from them. For instance, R_{ct} increases from 3.34×10^{-4} MΩ cm^2 in areas far from particles to 10^{-3} MΩ cm^2 close to them. The increased passivity of the surrounding matrix observed from local impedance measurements will be discussed by surface analysis in Section 3.4. The galvanic coupling between constituent particles (cathodic sites) and the surrounding matrix (anodic site) explains the increased passivity behaviour of the adjacent matrix zone. Similar mechanisms were proposed for AA2024-T351 in 0.1 M Na_2SO_4 + 0.001 M NaCl solution [24]. The only difference between the two alloys is that a deep trench was observed at the matrix–constituent particle interface on AA2024-T351 [24] whereas no trench was clearly observed on AA2050-T8 after a 25-min immersion in 0.1 M NaCl at OCP.

In both cases, the CPE exponents were close to unity. It should be mentioned that the CPE exponents decreased slightly with decreasing distance from constituent particles. The CPE coefficients were of the same order of magnitude in both cases.

3.4. Surface analysis after mechanical polishing

FE-SEM/EDS observations performed after immersion at OCP for 25 min revealed that sites containing large constituent particles were preferentially oxidised (Fig. 5). Some sites were slightly oxidised, as shown in Fig. 5(a). An FE-SEM/EDS analysis indicated that on average, the matrix (around constituent particles and close to them) contains the same quantity of copper as prior to immersion (approximately 2 at.%). A small amount of iron (0.13 at.%) and manganese (0.66 at.%) was detected in the immediate vicinity of constituent particles, suggesting that these two elements were redeposited during immersion. These elements were not detected in the matrix after polishing (values given in Section 3.1). Oxygen was preferentially absorbed in constituent particles (18 at.%) and in the matrix surrounding these particles (8.51 at.%). Only 2 at.% of oxygen was detected in areas of the matrix far from constituent particles. Increased passivity in areas of the matrix adjacent to constituent particles was then observed. These results confirm those that were obtained from electrochemical impedance measurements (Section 3.3).

Other sites were strongly oxidised. An FE-SEM/EDS analysis of the oxide layer formed around constituent particles (Fig. 5(b)) revealed the following composition: 48.7 at.% O, 43 at.% Al, 5.05 at.% Cu, 4 at.% Mn, 1.95 at.% Fe and 0.2 at.% Cl. Therefore, aluminium oxide or hydroxide first formed around constituent particles before covering them completely (Fig. 5(c)). These surface observations confirm that constituent particles in the 2050-T8 aluminium alloy behave as cathodic sites.

3.5. Electrochemical impedance measurements after ageing in air

To determine the effect of ageing in air for three months, local impedance measurements were performed on the untreated surface, as shown in Fig. 6(a) and (b). The evolution observed at sites containing the matrix was very similar to that at sites containing

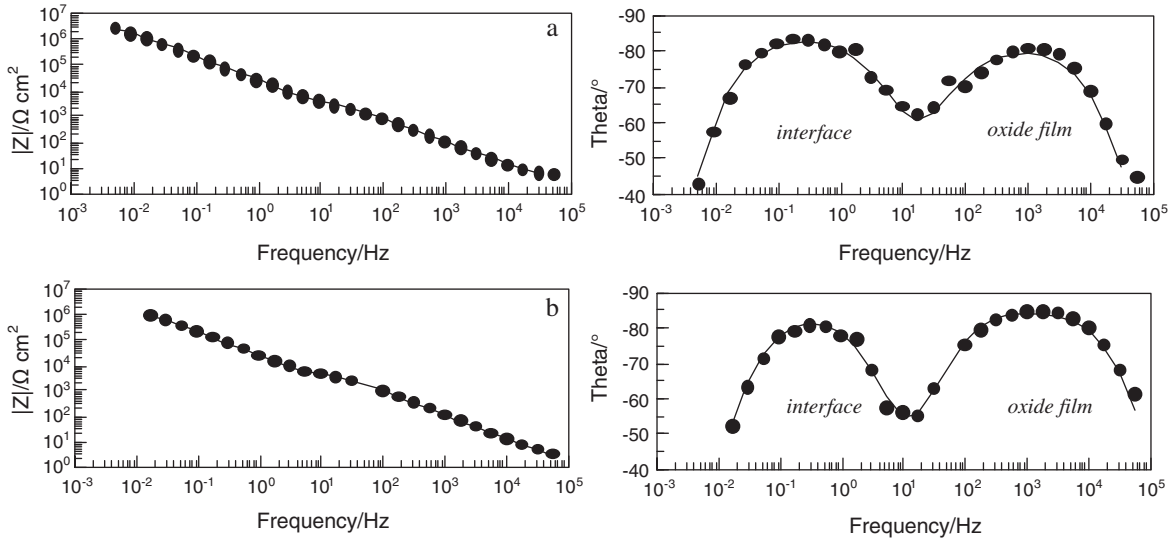

Fig. 6. Local electrochemical impedance diagrams (Bode representation) obtained on the untreated surface. Investigated sites contain the (a) matrix and (b) the matrix with constituent particles. Experiments were conducted after immersion of AA2050-T8 in 0.1 M NaCl at the OCP value for 25 min using 50 μm diameter capillaries. The lines represent the model data corresponding to the equivalent circuit in Fig. 3(c).

the matrix with constituent particles. Two capacitive loops were once again clearly visible. Ageing in air gave rise to an increase in the charge transfer resistance. This was clearly observed at sites with constituent particles (values ranging from 10^{-3} MΩ cm^2 to 1 MΩ cm^2, as shown in Table 2). A small increase of the oxide film resistance was also observed. The other numerical parameters (CPE coefficients and exponents) remained relatively constant.

It is well known that the surface film formed on pure aluminium and aluminium alloys consists of two sub-layers. The inner sub-layer, so-called the compact barrier layer, is amorphous. Its thickness is about 1 nm and is roughly the same, regardless of the ageing period (ageing in the laboratory at 25 °C for periods from one week to several years) [25]. On the other hand, the outer hydroxide sub-layer is porous and less protective than the barrier sub-layer. The thickness and the chemical composition of the outer sub-layer depends on the physical–chemical conditions during ageing (like humidity, temperature, etc.) [25,26]. It was shown [25] the thickness of the outer sub-layer increases with ageing in air for several years. Therefore, one may assume that changes observed in the charge transfer resistance by means of LEIS are related with the thickening of the outer sub-layer. On the other hand, small evolution of the oxide film resistance may be attributed to the inner oxide which is not significantly affected.

3.6. Electrochemical impedance measurements after LSP treatment

The effects of LSP were determined by comparing these values with the results obtained for the LSP-treated surface. Local impedance measurements were then performed on the LSP-treated surface.

Fig. 7(a) shows the Bode diagrams obtained for the matrix using 50 μm diameter capillaries. The two capacitive loops that were previously observed cannot be distinguished from impedance spectra. Numerical values of components derived from the fitting of experimental diagrams are reported in Table 2. It

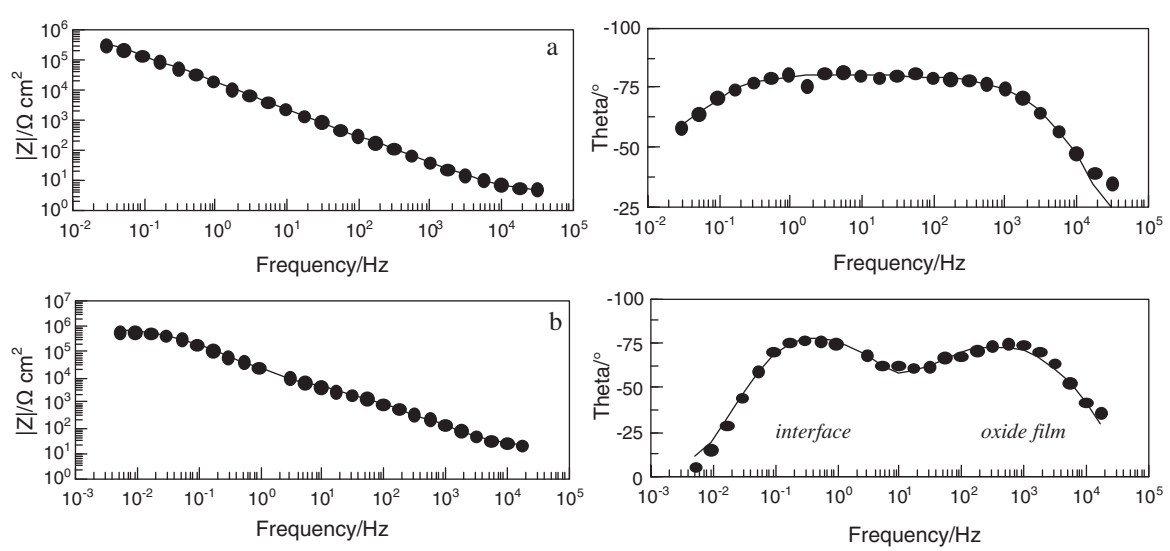

Fig. 7. Local electrochemical impedance diagrams (Bode representation) obtained on the LSP treated surface. Investigated sites contain the (a) matrix and (b) the matrix with constituent particles. Experiments were conducted after immersion of AA2050-T8 in 0.1 M NaCl at the OCP value for 25 min using 50 μm diameter capillaries. Lines represent the model data corresponding to the equivalent circuit in Fig. 3(c).

was found that the charge transfer and oxide film resistances increased sharply to approximately 0.35 MΩ cm^2 and 1 MΩ cm^2, respectively, as opposed to approximately 1.9×10^{-3} MΩ cm^2 and 4.2×10^{-3} MΩ cm^2, respectively, after ageing in air. By contrast, the CPE coefficients remained relatively unchanged. Therefore, LSP had significant effects on the electrochemical behaviour of the matrix. Note that surface defects formed in the matrix by the LSP treatment had nearly no influence on the impedance diagrams.

Two capacitive loops were once again observed at sites containing the matrix with constituent particles, as shown in Fig. 7(b). Table 2 shows that there were no changes with respect to the numerical values of components found after ageing in air (untreated surface). For instance, the oxide film and charge transfer resistances were once again approximately 2.9×10^{-3} MΩ cm^2 and 1 MΩ cm^2, respectively. Therefore, LSP has nearly no influence on the electrochemical behaviour of sites containing constituent particles.

At both types of sites (matrix and matrix with constituent particles), the CPE coefficients were lower (values of approximately 0.86 in Table 2) than they were after polishing or ageing in air (values of 0.9 shown in Table 2). The CPE behaviour observed in Fig. 7(a) and (b) can be attributed to time constant distributions either across the electrode area (involving only a two-dimensional surface) or along the axis normal to the electrode surface (involving a three-dimensional aspect of the electrode) [27]. A 2D distribution may arise from surface heterogeneities such as grain boundaries, crystal facets on a polycrystalline electrode, or other surface property variations. CPE behaviour may also arise from a 3D variation in properties. Such variability may be attributed to changes in the conductivity of oxide layers [28–30] or in porosity or surface roughness [31,32]. After LSP treatment, the CPE behaviour and the decrease in the CPE coefficients were attributed to the increase in surface roughness (from 4 nm after polishing to 9 nm after LSP).

4. Conclusions

Local electrochemical impedance spectroscopy (LEIS) was used to study the micro-electrochemical behaviour of AA2050-T8 alloy in sodium chloride solution. The influence of LSP and ageing in air on the passive properties of specimens has been investigated at the microscale. It has been shown that ageing in air leads to a significant increase of the charge transfer resistance and a small increase of the oxide film resistance (both at sites containing the matrix and at those containing the matrix with constituent particles). The increase of the corrosion resistance of samples after ageing in air was related with changes of the structure of the oxide film. By contrast, LSP leads to a sharp increase of the charge transfer and oxide film resistances at sites containing the matrix. This was attributed to the development of compressive stresses during LSP. LSP has nearly no influence on the electrochemical behaviour of sites containing constituent particles.

Acknowledgement

This work was supported by the Agence Nationale de la Recherche (ANR, France) under the project #BLAN07-2_185038 (CAPSUL).

References

[1] K. Nisancioglu, J. Electrochem. Soc. 137 (1990) 69.
[2] E.Mc. Cafferty, J. Electrochem. Soc. 150 (2003) B238.
[3] J.L. Searles, P.I. Gouma, R.G. Buchheit, Metall. Mater. Trans. 32A (2001) 2859.
[4] N. Birbilis, R.G. Buchheit, J. Electrochem. Soc. 152 (2005) B140.
[5] J.O. Park, C.H. Paik, R.C. Alkire, J. Electrochem. Soc. 143 (1996) L174.
[6] A. Davoodi, J. Pana, C. Leygraf, S. Norgren, Appl. Surf. Sci. 252 (2006) 5499.
[7] M.M. Lohrengel, A. Moehring, M. Pilanski, Electrochim. Acta 47 (2001) 137.
[8] M.M. Lohrengel, A. Moehring, M. Pilanski, Fresenius J. Anal. Chem. 367 (2000) 334.
[9] A.W. Hassel, M.M. Lohrengel, Electrochim. Acta 42 (1997) 3327.
[10] H. Böhni, T. Suter, F. Assi, Surf. Coat. Technol. 130 (2000) 80.
[11] T. Suter, R.C. Alkire, J. Electrochem. Soc. 148 (2001) B36.
[12] F. Andreatta, M.M. Lohrengel, H. Terryn, J.H.W. de Wit, Electrochim. Acta 48 (2003) 3239.
[13] C. Rodopoulos, C.S. Romero, S.A. Curtis, E. De Los Rios, P. Peyre, J. Mater. Eng. Perform. 12 (2003) 414.
[14] A.H. Clauer, J.H. Holbook, B.P. Fairand, Shock Waves and High-Strain-Rate Phenomena in Metals, Concepts and Applications, Plenum, New York, 1981, p. 675.
[15] X. Liu, G.S. Frankel, B. Zoofan, S.I. Rokhlin, Corros. Sci. 46 (2004) 405.
[16] H. Krawiec, V. Vignal, Z. Szklarz, J. Solid State Electrochem. 13 (2009) 1181.
[17] H. Bohni, T. Suter, F. Assi, Surf. Coat. Technol. 130 (2000) 80.
[18] H. Krawiec, V. Vignal, R. Akid, Surf. Interface Anal. 40 (2008) 315.
[19] H. Krawiec, V. Vignal, R. Akid, Electrochim. Acta 53 (2008) 5252.
[20] V. Hauk, Structural and Residual Stress Analysis by Nondestructive Methods, Elsevier, Amsterdam, 1997.
[21] Ph. Lequeu, K.P. Smith, A. Daniélou, J. Mater. Eng. Perform. 19 (2010) 841.
[22] A. Raveh, Z.K. Tsameret, E. Grossman, Surf. Coat. Technol. 88 (1996) 103.
[23] G. Alcala, S. Mato, P. Skeldon, G.E. Thompson, P. Bailey, T.C.Q. Noakes, H. Habazaki, K. Shimizu, Corros. Sci. 45 (2003) 1803.
[24] L. Lacroix, L. Ressier, C. Blanc, G. Mankowski, J. Electrochem. Soc. 155 (2008) C131.
[25] M.S. Hunter, P. Fowle, J. Electrochem. Soc. 103 (1956) 482.
[26] H.P. Godard, J. Electrochem. Soc. 114 (1967) 354.
[27] V.M.W. Huang, V. Vivier, M.E. Orazem, N. Pébère, B. Tribollet, J. Electrochem. Soc. 154 (2007) C81.
[28] L. Young, Trans. Faraday Soc. 51 (1955) 1250.
[29] L. Young, Anodic Oxide Films, Academic Press, New York, 1961, p. 10.
[30] C.A. Schiller, W. Strunz, Electrochim. Acta 46 (2001) 3619.
[31] R. Jurczakowski, C. Hitz, A. Lasia, J. Electroanal. Chem. 572 (2004) 355.
[32] T. Pajkossy, Solid State Ionics 176 (2005) 1997.